N. Taymourtash, A. Zanotti, G. Gibertini, G. Quaranta
Unsteady Load Assessment of a Scaled-Helicopter Model in a Ship Airwake
Aerospace Science and Technology, In press-Published online 26/04/2022
doi:10.1016/j.ast.2022.107583

Unsteady Load Assessment of a Scaled-Helicopter Model in a Ship Airwake

Neda Taymourtash[a,b,1,*], Alex Zanotti[a,2], Giuseppe Gibertini[a,3], Giuseppe Quaranta[a,4]

[a] *Department of Aerospace Science and Technology, Politecnico di Milano, Milan, Italy*
[b] *Aerospace Sciences Division, James Watt School of Engineering, University of Glasgow, Glasgow, UK.*

Abstract

The paper presents the results of wind tunnel tests to measure unsteady aerodynamic loads on a scaled-helicopter operating in the airwake of a generic frigate model. Rotor loads were measured by a six-axis dynamic balance in a stern landing maneuver simulated by trimming the rotor along a sloped descent trajectory towards the landing spot. The measures allowed to identify not only the average loads but also the frequency spectrum in the range of interest for flight mechanics. The results indicate that for the three tested wind directions, including headwind, 30° and 60° from the port-side, moving towards the landing spot the unsteadiness is increased. The rate of amplification of the loads for the trajectories not aligned with the wind is significantly higher compared with those measured in the headwind test. Furthermore, a fully dynamic landing maneuver was compared with the sequence of trimmed measures to evaluate the effect of the approach velocity of the helicopter on unsteady loads. A notable reduction in the unsteadiness of the pitch moment was found, while the unsteady thrust and roll moment were more comparable between static and dynamic tests.

*Corresponding author
Email addresses: Neda.Taymourtash@polimi.it (Neda Taymourtash), Alex.Zanotti@polimi.it (Alex Zanotti), Giuseppe.Gibertini@polimi.it (Giuseppe Gibertini), Giuseppe.Quaranta@polimi.it (Giuseppe Quaranta)
[1] PhD Student
[2] Assistant Professor
[3] Associate Professor
[4] Full Professor

Keywords: Wind Tunnel Test, Helicopter, Dynamic Interface, Ship Landing, Unsteady Aerodynamic

---

Nomenclature

c	=	Blade chord (m)
C_P	=	Pressure coefficient, $2(P - P_\infty)/(\rho U_\infty^2)$
C_T	=	Thrust coefficient, $T/\left(\rho\Omega^2 R^2 A\right)$
C_M	=	Pitch moment coefficient, $M/\left(\rho\Omega^2 R^2 AR\right)$
C_L	=	Roll moment coefficient, $L/\left(\rho\Omega^2 R^2 AR\right)$
R	=	Rotor disc radius (m)
Re_{TIP}	=	Reynolds Number at blade tip, $\Omega Rc/\nu$
U_∞	=	Free-stream wind velocity magnitude (m/s)
(X, Y, Z)	=	Absolute reference system
(x, y, z)	=	Rotor reference system
Z_{ref}	=	Height of the reference Pitot probe (mm)
μ	=	Advance ratio, $U_\infty/(\Omega R)$
σ_x	=	RMS value of x, $\int_{f1}^{f2} PSD(x)df$
PSD	=	Power Spectral Density
HW	=	Headwind
R30	=	Red wind from 30°
R60	=	Red wind from 60°
DI	=	Dynamic Interface
GVPM	=	Galleria del Vento Politecnico di Milano
RMS	=	Root Mean Square
SHOL	=	Ship Helicopter Operational Limitations

1. Introduction

Shipboard operations are among the most challenging tasks for the helicopter pilots. During the launch and recovery phases, the flow field over the

ship deck becomes highly unsteady and turbulent, especially when the helicopter is operating in close proximity to the superstructure of the ship. A strong aerodynamic interaction between rotor inflow and airwake of the ship, in addition to the deck motion in rough sea states, unsteady wind profile, and the requirement to operate in a confined area, and often with degraded visibility, are the main challenges in the helicopter-ship Dynamic Interface(DI) environment [1]. The combination of these elements results in a significantly increased level of pilot workload [2], and negatively affects the performance and handling qualities of the aircraft.

Safety analysis for such demanding missions is usually performed through a series of at-sea trials which are inherently hazardous and extremely expensive. Furthermore, each combination of ship-helicopter should be tested for a full range of Wind-Over-Deck (WOD), which is difficult to obtain in the period of testing, to find the envelope of safe operation, so-called Ship-Helicopter Operational Limitations (SHOL) [3]. Consequently, the development of the helicopter-ship DI simulation is considered as a viable solution which reduces the cost and hazards of time-consuming at-sea test campaigns [4]. Such a simulation tool could be used to find the optimal trajectory for a safe landing, to design and test new flight control systems (FCS), and for training pilots for the dynamic interface environments. FCS with the capability to be used for this peculiar maneuver are being developed for helicopters [5], or unmanned vehicles that are operated from ships [6, 7]. In all cases, a detailed knowledge of the disturbances introduced by the flow field is essential for the correct design.

For SHOL testing, high levels of fidelity are required for DI simulation which is decomposed into the models and subsystems and further decomposed into the individual elements. Then, the overall fidelity is measured from a quantitative description of fidelity for each constituent element [8, 9]. In this regard, airwake modeling is recognized as a crucial element that strongly impacts the overall fidelity. The importance of including the unsteady airwake, in addition to the steady components, was evaluated by performing piloted simulation to obtain the SHOL envelope [10]. Regarding the pilot ratings and the driven SHOL, it

was concluded that "the lack of unsteadiness in the airwake [...] resulted in lower workload than normally experienced". This finding led to the development of several researches assessing the level of unsteadiness in the flow field of helicopters immersed in the airwake of the ship using numerical or experimental setup [11, 12, 13]. With the majority of the airwake energy concentrated in the bandwidth of 0.2–2.0 Hz, as shown in [14], the unsteadiness of the flow field directly affects the handling qualities since the typical pilot closed-loop bandwidth goes up to a maximum cross-over frequency of 1.6 Hz (10 rad/s) due to the intrinsic neuromuscular lags, as identified by McRuer in [15]. Also, it has been demonstrated that the correct representation of the time-accurate disturbances is important in replicating the workload experienced by the pilots [16, 17].

One of the main challenges involved in the modeling of the flowfield is the mutual interaction between the ship airwake and the helicopter. The aerodynamic loads of the helicopter are modified due to the presence of the ship airwake, but in turn, the flowfield is changed by the wake of the rotor creating a complex feedback connection between the two flows. Although the most representative approach is the development of a fully-coupled simulation in which the aerodynamic solver and flight dynamics code should be run simultaneously with the communication between two codes, due to the excessive computational cost, currently this approach cannot support the real-time DI simulations [18, 19, 20, 21]. Another approach to analysing the unsteadiness involved in this mutual interaction is to perform the scaled experiments with the helicopter model operating in the airwake of the ship, while the wind speed and direction can be set according to the SHOL diagram.

Towards this aim, few experimental setups are developed at sub-scale to evaluate the unsteady loading in different phases of the landing maneuver and with respect to various wind conditions. One of the first experimental investigations was done by Zan at Aerodynamic Laboratory, National Research Council of Canada [22]. The initial experiments were conducted with an isolated powered rotor mounted on a sting capable of moving over the deck of a 1:50 scale model of

the Canadian Patrol Frigate (CPF). With a fixed incidence setting on the blades, the time-averaged thrust was measured on a dynamic balance. This study has demonstrated that the reduced inflow to the rotor, due to the ship airwake, can significantly decrease rotor thrust up to 15%. Following this campaign, another setup was developed aimed at evaluation of the unsteady side-force, yawing moment, and drag force applied on a rotor-less Sea King fuselage immersed in the turbulent airwake of CPF [23]. To quantify the unsteady loading, Power Spectral Densities (PSD) were calculated from the time histories of the measured aerodynamic loads, and the square root of the integral over the bandwidth of 0.2 to 2 Hz was taken as the measure of unsteadiness. Across this frequency range, the magnitude of the spectrum represents a portion of the pilot workload associated with response to the airwake turbulence. Consequently, a reasonable correlation was found between RMS loading and pilot workload obtained from flight tests. The setup was further modified by adding a 1:50 scale rotor of Sea King to account for the effect of rotor downwash on the fuselage loading [24]. It was shown that in most cases the unsteady loading increased with the presence of the rotor downwash. Also, the level of unsteadiness at different positions over the deck and in different wind speeds was changed compared with the rotor-less case.

Another setup was designed and developed at the University of Liverpool, UK, by Wang et al. to measure the unsteady forces and moments imposed by the airwake of a generic ship on a 1:54 scale model of Merlin AW-101 helicopter [12]. The setup, specially designed for testing in a water tunnel, was used to simulate two WOD conditions, including headwind and wind coming with a direction of 45° from the starboard side, conventionally indicated as Green45, and the measurements were conducted at fixed positions along the flight path of a landing maneuver [25]. Time-averaged measurements identified a region of thrust deficit in headwind and a pressure wall in the 45° wind angle. The unsteady loading was also compared in terms of severity and showed higher RMS loading in Green45 and particularly through the lateral translation phase. The setup has been used also to investigate the potential benefits of aerodynamic

modifications to the ship geometry [26]. Various modifications were proposed and many were found effective in reducing the RMS forces and moments. In particular, the promising design concepts were a side-flap and notch modification which both showed consistent improvements of 25-50% in unsteady loading.

More recently, a setup was developed at Politecnico di Milano to study the aerodynamic interaction between a 1:13 scaled-helicopter model and Simple Frigate Shape 1, as a generic ship geometry [27]. Initially, a series of wind tunnel tests were performed to characterise the airwake of the isolated ship in different WOD conditions, with and without Atmospheric Boundary Layer (ABL), using Particle Image Velocimetry (PIV) technique. Then, the time-averaged aerodynamic loads of the rotor were measured, while the helicopter was placed in a series of points representative of a stern landing trajectory and a vertical descent over the landing spot. In that case, a rotor without a swashplate was used and the blades were rigidly attached to the hub with a fixed pitch angle, so no load trimming was allowed. Steady load measurements were performed in two WOD conditions, including headwind and Red30, where red indicates a wind coming from the port side, in addition to a no-wind test. Variation of the mean aerodynamic loads showed a strong ground effect while moving towards the deck. Furthermore, a significant reduction of the pitch moment was identified due to the interaction between the downwash produced by the recirculation zone and the inflow of the rotor.

As a further step towards DI simulation, this research aims to study the unsteady aerodynamic loading of a scaled-helicopter operating in the airwake of a generic ship model. Towards this goal, the setup introduced in [27] has been substantially improved so that a landing trajectory can be simulated while trimming the rotor to obtain a specific set of aerodynamic loads. The desired trim loads can be achieved by applying collective and cyclic commands through a swashplate mechanism implemented in the model. Taking advantage of this new setup, a series of wind tunnel tests have been conducted to investigate the effect of wind speed and direction on unsteady rotor loads. Three different wind directions were selected, including headwind, Red30, and Red60. Furthermore,

the tests in HW and Red30 were performed at two different wind speeds for each direction. After trimming the rotor at different positions with respect to the deck, aerodynamic loads were measured to evaluate the unsteadiness over a frequency range of interest, corresponding to the low-frequency bandwidth of 0.2-2 Hz in full-scale. Moreover, the new setup was exploited to simulate "Dynamic Landing" by setting a constant approach velocity for the helicopter to perform the landing maneuver. So, in addition to the effect of three main parameters, including rotor position, velocity, and direction of the wind on the unsteady loading of the rotor, the effect of dynamic landing will be also presented and discussed throughout the following sections.

2. Experimental Setup

The experiments were conducted in the large test chamber of the Wind Tunnel of Politecnico di Milano (GVPM) with 13.84 m wide, 3.84 m high, and length of 35 m. Figure 1 shows the complete setup mounted inside the test chamber. The setup consists of a 4-bladed helicopter and a simplified ship model. The helicopter model was held by a horizontal strut connected to a system of two motorised orthogonal sliding guides which can change the relative position of the helicopter in both vertical and longitudinal directions. A fixed reference frame is defined to introduce the test points, which represent the position of the rotor hub center with respect to the ship. The XZ plane of the reference frame, as represented in Fig. 2(a), is aligned with the longitudinal symmetry plane of the deck. All the setup was mounted on the large turning table of the test section with a diameter of 13 m, so that the effect of wind direction could be tested as well.

No ABL was considered in this experiment, differently from the test performed in Ref. [27]. The free stream flow in the tunnel is representative of a low-turbulence uniform velocity profile, with a boundary layer thickness of 0.15 m (approximately 40% of the height of the flight deck) and a mean turbulence level of 2%. As a reference point to measure the free stream velocity, a Pitot

probe was mounted on top of the superstructure, 180 mm above and 90 mm upstream of the mast. In each test, the probe was adjusted to have the static port aligned with the wind direction.

Figure 1: Test setup mounted inside the test chamber of GVPM.

2.1. Ship Model

The ship model is a 1:12.5 scale model of Simple Frigate Shape 1 which is a highly simplified but representative ship geometry, developed as a part of an international collaboration in which Canada, Australia, New Zealand, UK, and USA evaluated the ability of CFD codes to simulate complex airwakes [28].

The SFS1 model consists of a rectangular prism with a step on its rear and another prism on top which is acting as a ship superstructure, as represented in Fig. 2(a), reporting the main dimensions of the model. The landing point of the helicopter model was placed on the center of the turning table, thus the ship can be rotated to both sides, while the landing point remains fixed with respect to the boundaries of the test section.

The flight deck and hangar wall were equipped with 77 and 35 pressure taps, respectively. The pressure measurements were performed using four low-range 32-ports pressure scanners embedded inside the ship model. The declared accuracy of the pressure scanners led to an estimated uncertainty for the pressure

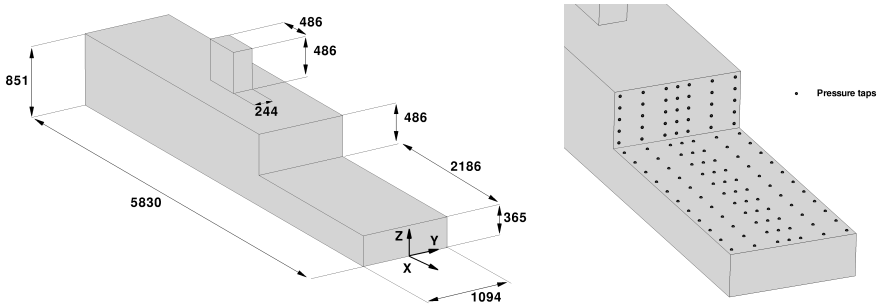

(a) Dimensions (in mm) (b) Pressure taps

Figure 2: Sketch of the 1:12.5-scale model of SFS1 equipped with pressure taps.

coefficient of approximately ±0.15%, while previous experience and some tests carried out before the experiment showed an uncertainty of less than 0.1%.

2.2. Helicopter Model

The helicopter model consists of a fuselage and a rotor which has four untwisted and untapered rectangular blades, made of carbon-fiber composite materials with NACA0012 airfoil. The rotor, with a diameter of 970 mm, includes a complete swashplate mechanism so that collective and cyclic commands can be applied to the blades to trim the rotor while approaching the flight deck. A polycarbonate fuselage was manufactured with Fused Deposition Modelling (FDM) technique to be representative of a 1:10 scaled-model of Bo-105 as a generic medium size helicopter. The fuselage is mounted on an internal metallic structure housing a six-components strain gauge balance (Koris F6D-80e-60) and the driving motor system for the rotor. The balance, with a nominal accuracy of 0.5% of full range, was calibrated for maximum loads of ±60 N along the lateral and longitudinal axes, and ±120 N along the vertical axis measuring the thrust, and maximum moments of ±6 Nm. A series of static calibration tests were performed to identify the coupling between different axes of the load cell. The uncertainty of the measurement after applying the identified calibration matrix was found to be less than 2% for all six axes. Since the rotor is decoupled from the fuselage, the balance measurement is related to the aerodynamic

loads of the rotor. For this reason, all load measurements are expressed in the rotor reference frame, with the origin on the hub center, x axis from nose to tail, y lateral axis towards the starboard, and the z vertical axis pointing in the upward direction.

To verify the dynamic range of the balance a preliminary numerical model based on the nominal stiffness of the balance arms and the estimated mass and moments of inertia of the model has been used to ensure that all natural frequencies were above 40 Hz. Simple impulse responses made through hammer tests on the model installed on the wind tunnel supporting structure revealed that no balance natural frequencies were present below 40 Hz while a support natural frequency was present. This mode was characterized by a bending of the horizontal strut of the support system at 5.47 Hz. It was concluded that the dynamic response of the balance was suitable for measuring the helicopter model unsteady loads in tho whole range of interest i.e., between 0.95 and 9.5 Hz, excluding the effect of the bending mode that had to be filtered. This effect was removed by applying a physics-based method introduced in [29] which eliminates the spurious resonant peaks from the measured PSDs. In this approach, the frequency response of a single degree-of-freedom mechanical system, represented as a "mass-spring-damper" model with a known natural frequency at 5.47 Hz, is applied to the measured spectra, so that the unwanted peak and its local effect are removed. The resultant filtered spectra are then used for the unsteady analysis of the aerodynamic loads.

A brushless motor, with 3.3 kW continuous power was connected directly to the rotor shaft through a joint coupling. The rotor rotational speed was maintained in all tests using an Electronic Speed Controller (ESC) connected to the motor and recorded with the same sampling frequency as the balance loads so that the load coefficients can be calculated based on the instantaneous RPM of the rotor. The main dimensions of the helicopter model are reported in Fig. 3(a). Furthermore, the internal layout of the fuselage representing the arrangement of the motor, the balance, and other instruments is presented in Fig. 3(b).

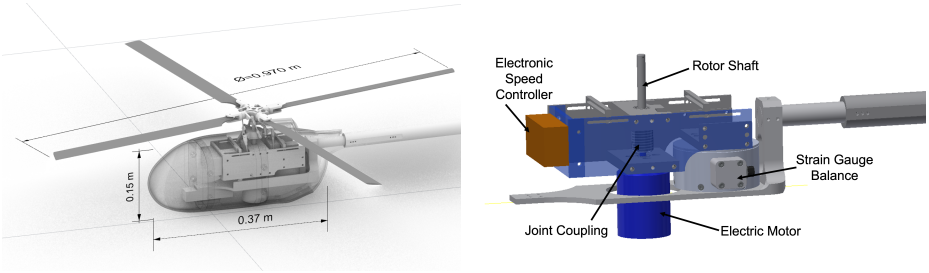

(a) Main dimensions of the helicopter model (b) Internal layout of the fuselage

Figure 3: Dimensions and layout of the helicopter model.

2.3. Scaling Parameters

The main scaling parameter applied to this investigation is to maintain the Strouhal number of the full-scale model. This matching requires the correct scaling of three parameters, including frequency, geometry, and free stream velocity. Considering Bo-105 as a generic medium-size helicopter, the geometric scale, based on rotor radius, is fixed at 1:10.1. The rotational speed of the rotor was selected high enough to increase the Reynolds and Mach numbers, while retaining the wind speed, as required by Strouhal similarity, within the limits of free stream velocity of the test section. Consequently, a frequency scale of 4.75:1 was fixed which leads to the velocity scale of 1:2.1. This velocity scale gives the ship-based Reynolds number in the range of 3.5×10^5 to 6.1×10^5 while testing in different wind speeds, which satisfies the minimum Reynolds number of 11000 for wind tunnel testing of sharp-edged bodies, like SFS1, to be insensitive to Reynolds number [30]. Some preliminary tests were performed to select a thrust level that could be maintained in all test conditions, while avoiding excessive operating temperature and power extraction from the electric motor, and overloading the mechanism of the swashplate that was not designed specifically for this test. Consequently, the resultant thrust coefficient is 60% of the full-scale value. It should be noted that the objective of this experiment is not to examine the loading characteristics of the Bo-105 helicopter. Instead, this setup has been developed to verify if the proposed experimental approach is an

effective instrument to study the steady and unsteady loading of a rotor operating in a fully-coupled environment. The load measurements then can be used to predict the variation of the rotor inflow due to the interaction with the ship airwake, which is more difficult to be measured especially in flight tests. Table 2 presents all parameters of the model compared with Bo-105.

Table 2: Parameters of the experimental model and Bo105.

Characteristic	Scaled Model	Bo105
Number of Blades	4	4
Rotor Radius (m)	0.485	4.91
Angular Speed (rad/s)	211	44.4
Blade Chord (m)	0.042	0.27
Free Stream Velocity (m/s)	4.8-8.4	10.3-18
Advance Ratio	0.047-0.082	0.047-0.082
Tip Mach Number	0.3	0.63
Tip Reynolds Number	2.9×10^5	3.9×10^6
Thrust Coefficient	0.0028	0.0046

3. Test Plan

A typical stern landing trajectory was defined including four points (P1 to P4) along a descent path with a slope angle of 15° towards the landing point. The point P0 was used as a check point to identify a position that is outside the influence of the ship airwake. It has been tested that no significant changes in controls required to trim the rotor were necessary at P0, with or without the presence of the ship model. Furthermore, three additional points (P5 to P7) were selected which are representative of a vertical descent over the deck. Figure 4 shows all the test points with the positions listed in Table 3. The coordinates are in the same reference frame introduced in Fig. 2(a).

To simulate the landing maneuver, the rotor was positioned at each point. Applying collective and cyclic commands, the rotor was trimmed to obtain a

specific level of thrust and zero in-plane moments. Then, trim commands were fixed and the acquisition of the loads was performed for 30 seconds with the sampling frequency of 100 Hz and repeated twice for each point.

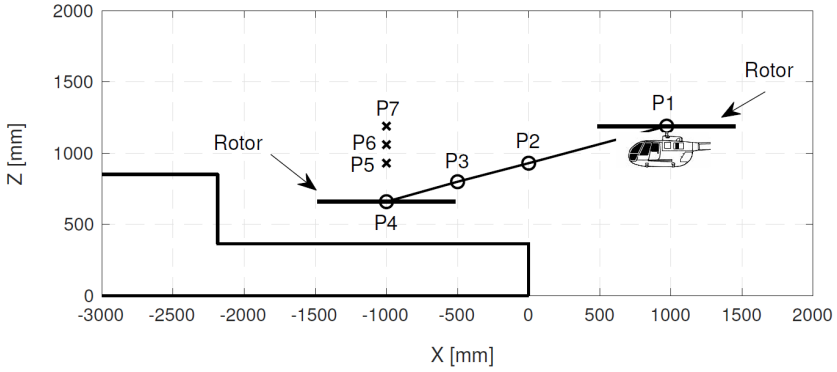

Figure 4: Side-view of the test points. Circles and crosses represent the position of the rotor center in stern landing and vertical descent, respectively.

Table 3: Coordinate of the test points in ship reference frame.

Test Point	X [mm]	Y [mm]	Z [mm]
P0	1940	0	1450
P1	970	0	1190
P2	0	0	930
P3	-500	0	800
P4	-1000	0	660
P5	-1000	0	930
P6	-1000	0	1060
P7	-1000	0	1190

As required by SHOL analysis, the test conditions were selected based on different wind speeds and directions. Five wind conditions were tested, including two velocities in Head Wind (HW), two velocities in Red Wind from 30° (R30), and one velocity in Red Wind from 60° (R60). Figure 5 shows the selected test conditions in full-scale values.

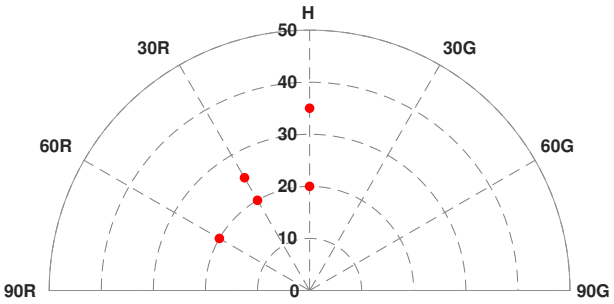

Figure 5: Selected test conditions (red dots) imposed on a typical SHOL diagram in full-scale (velocities in knots).

A second approach, called "Dynamic Landing" was tested for three wind conditions. In this approach, the helicopter is moving towards the landing point with a constant velocity, while the trim controls, obtained during the static tests for each point, are applied to the rotor. The predefined trajectory, starts with 5 seconds initial hover at P1, after descending towards P5 with a constant velocity of $0.1m/s$, it ends with 5 seconds hover at P4. Regarding the scaling parameters of the test, the selected approach velocity corresponds to a velocity of $1m/s$ with respect to the ship deck in full-scale, which is well representative of the final phase of a landing maneuver that is a low speed forward flight near the deck. Figure 6 shows the time history of the longitudinal and vertical position of the rotor during 30 seconds of the dynamic maneuver.

4. Results and Discussion

In this section, first the time-averaged aerodynamic loads are presented to verify that the trim objective in all test points and test conditions has been correctly obtained. Then, the analysis of the unsteady loads is presented and discussed in both time and frequency domains. It is notable that since the predominant effect of the unsteady airwake on the rotor loads is known to be along heave, pitch, and roll axes [14], in the following sections only thrust and in-plane moments are discussed.

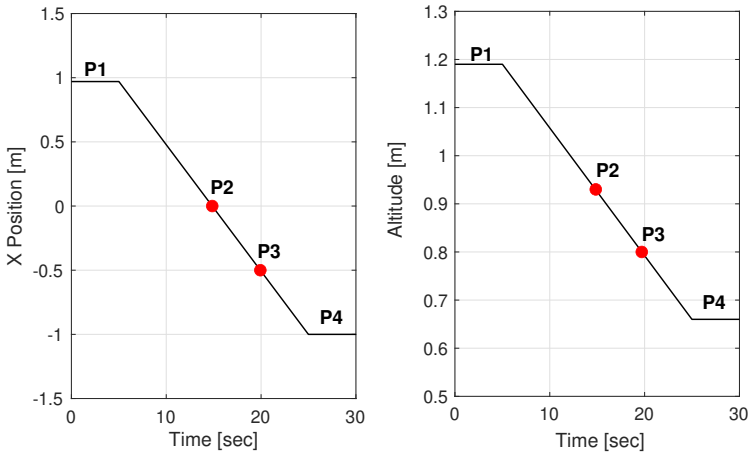

Figure 6: Time history of the longitudinal and vertical position of the rotor in dynamic landing test.

4.1. Rotor trim

Moving towards the landing area, the recirculation created behind the hangar wall and its extension over the deck will cause to a rotor with constant collective and cyclic blade pitch angles the development of a nose-down pitching moment and a decreasing thrust [27]. The objective of the trim procedure in all test conditions presented in Fig. 5, and for all test points listed in Table 3, was to obtain a thrust coefficient of 0.0028 and zero in-plane moment coefficients, which could be achieved by applying collective and cyclic controls through the swashplate. Following the approach used by Lee and Zan [24], a tolerance of $\pm 10\%$ was considered a reasonable target to effectively use the wind tunnel time and to avoid over-running the electric motor. Figure 7(a) compares the average of thrust coefficient over 30 seconds of acquisition and two repetitions for each point; it confirms that in all tests, the thrust was kept within the range of $\pm 10\%$ of the trim objective. For the roll and pitch moments, it has been considered acceptable the value of 0 ± 0.7 Nm, that is 25% of the maximum moment obtained during no trim tests. As shown in Figs.7(b) and 7(c), these limits correspond to a moment coefficient of $\pm 1.55 \times 10^{-4}$, and they have been

fairly respected in all tests.

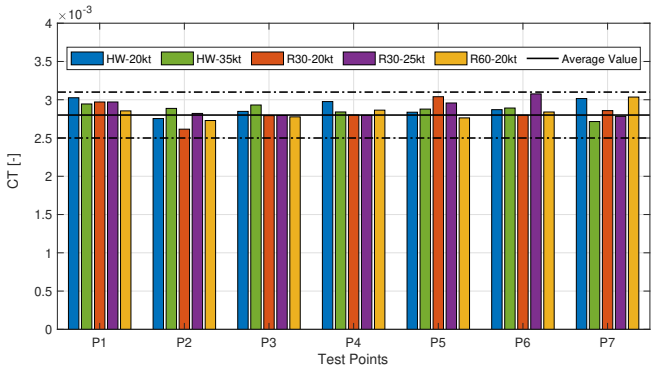

(a) Thrust Coefficient

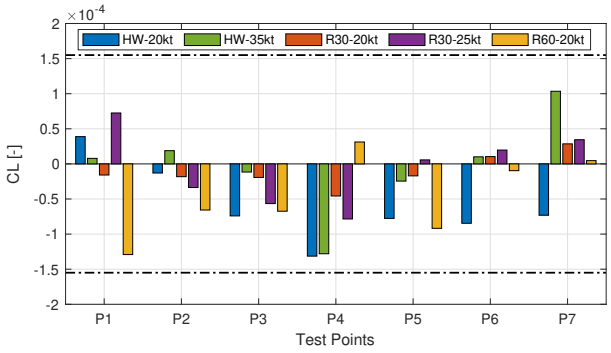

(b) Roll moment coefficient

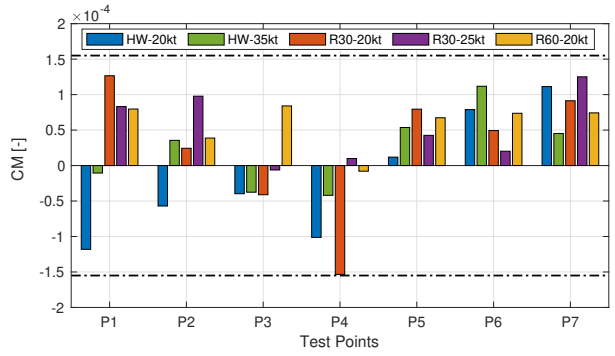

(c) Pitch moment coefficient

Figure 7: Comparison of time-averaged trimmed load coefficients for all test points. The dashdotted lines represent the tolerance limits used for trimming the loads.

As a complementary analysis for the trim tests, the contours of the pressure coefficient over the deck and hangar wall are presented for three wind directions with the same speed, both while the rotor wake is not influencing the pressure distribution over the deck in Fig.8, and while the rotor is positioned at P3, P4, and P5 in Fig.9. At these positions, regarding the proximity of the rotor to the deck, the effect of the rotor wake on the pressure field is more significant. To allow to appreciate the modification induced by the presence of the rotor, the pressure measurements with the helicopter model placed at P0, where there are no mutual influences, are shown as well. It should be mentioned that the pressure contours represent the mean values over the 30 seconds of acquisition while performing the trim tests at each point. A high-pressure region caused by the wake impingement is evident when the rotor is positioned close to the flight deck at landing spot (P4), however, with the wind coming from the port side, especially in R60 where the WOD is less deflected due to the interaction with the hangar wall, this high-pressure zone is moved back and towards the starboard side of the deck. The extension of the low-pressure region towards the port side is also noticeable in both red wind conditions. A similar topology is observed when the rotor is placed at P3 and P5, however with lower pressure peaks due to higher altitude over the deck.

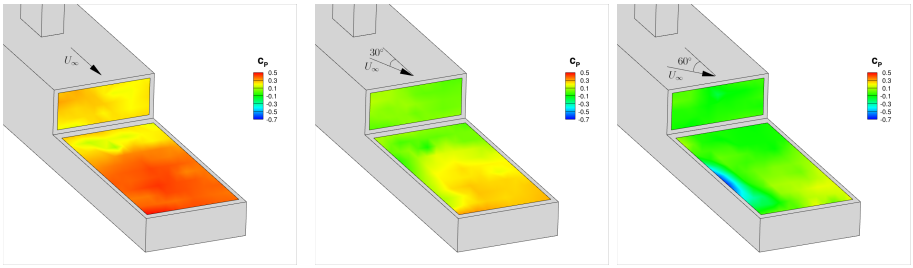

(a) P0, HW (b) P0, R30 (c) P0, R60

Figure 8: Comparison of the pressure coefficient contours in HW, R30 and R60 with helicopter at position P0, where pressure on the deck is not significantly affected.

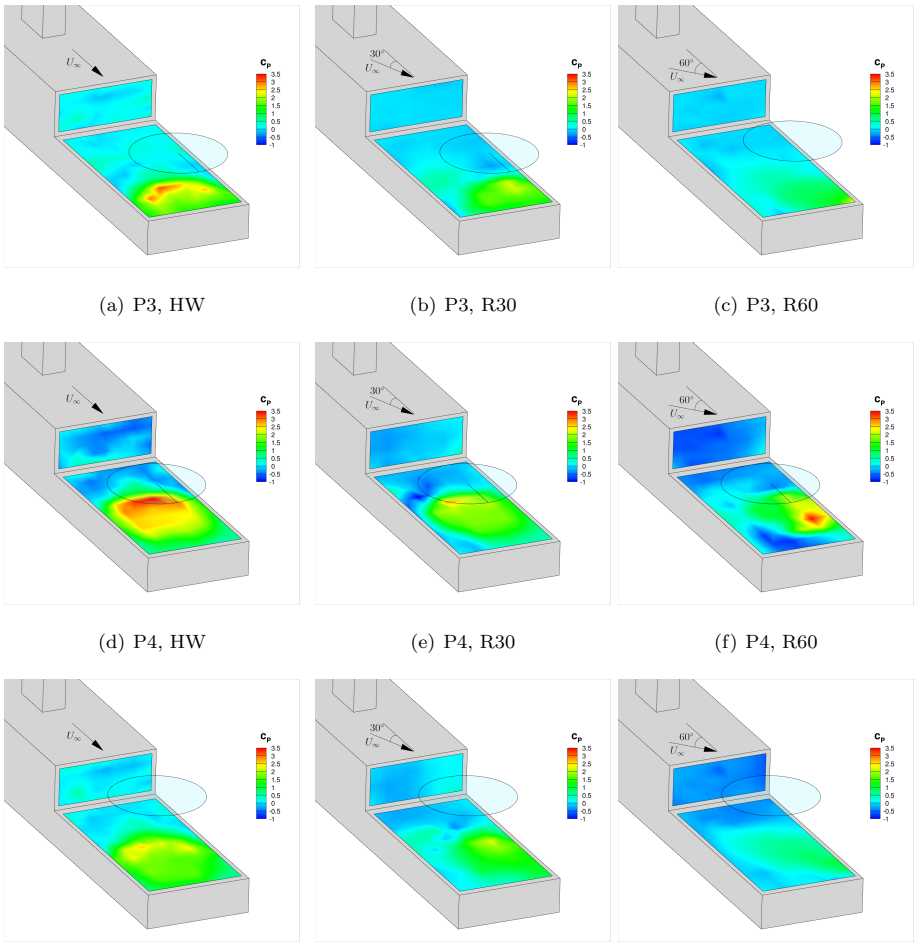

(a) P3, HW (b) P3, R30 (c) P3, R60

(d) P4, HW (e) P4, R30 (f) P4, R60

(g) P5, HW (h) P5, R30 (i) P5, R60

Figure 9: Comparison of the pressure coefficient contours in HW, R30 and R60 with rotor placed at different positions over the deck. For point P0 the color scale used for pressure coefficient is different.

4.2. Unsteady loads

To evaluate the unsteadiness of the aerodynamic loads in different positions and wind conditions, first, the time histories are compared and then a more quantitative comparison in the frequency domain is presented. To have a better presentation of the time histories, all measured signals were filtered by a low-pass filter with a cut-off frequency of 15 Hz. Since the bandwidth of interest for unsteady loads is significantly lower than this frequency, the filtering does not affect the results of the unsteady analysis. Figure 10(a) compares the time history of the load coefficients, in two HW tests while the rotor is placed at P4. It is clear that in all three axes, the fluctuations are notably increased when moving to higher wind speed. The comparison of the effect of wind direction at the same point, presented in Fig. 10(b), shows slightly more disturbance in R60 with respect to HW test. However, this effect is not as significant as the effect of wind speed.

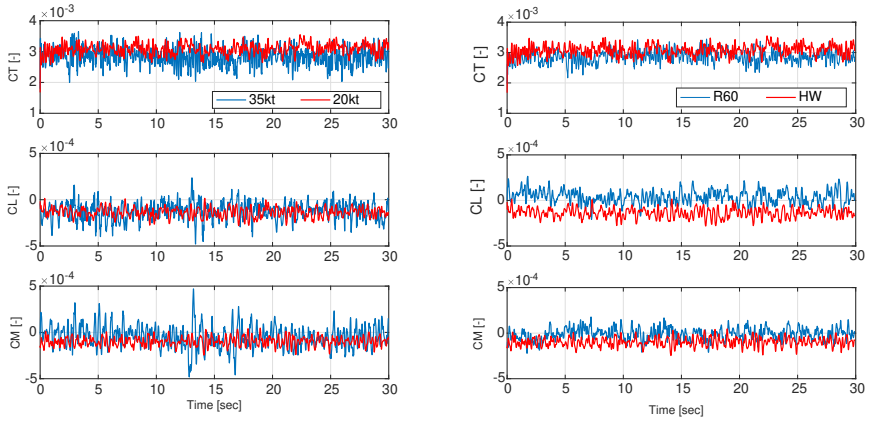

(a) HW - P4 (b) 20kt - P4

Figure 10: Time histories of aerodynamic load coefficients at P4 - Effect of wind velocity and direction.

Figure 11 which compares the effect of the position of the rotor over the deck on the aerodynamic loads. Initial and final points of the stern trajectory (P1 and P4) are selected for this comparison. The time history of all three load

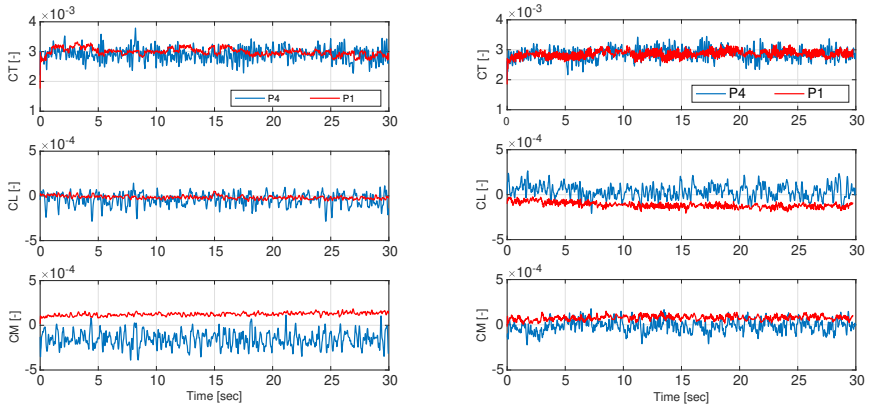

(a) R30 - 20kt (b) R60 - 20kt

Figure 11: Time histories of aerodynamic load coefficients at P4 - Effect of rotor position in R30 and R60.

coefficients indicates that moving towards the landing area, the amplitude of the fluctuations are remarkably increased in both R30 and R60 conditions.

To quantify the unsteady aerodynamic loading of the rotor, the method proposed by Lee and Zan [23, 24] is implemented. In this approach, first, the PSD is calculated from the measured time-histories of the loads. Then, the square-root of the integral in the bandwidth of interest is considered as a measure of unsteadiness, so-called RMS loading. The low-frequency content of the airwake, in the bandwidth of 0.2-2 Hz, directly impacts the workload of the pilot. Therefore, the integral should be calculated over the equivalent full-scale bandwidth , which needs to be correctly mapped into the frequency scale of the test. Figure 12 shows an example of a PSD calculated in both full and test frequency scales. Regarding the frequency scale of 1:4.75, the bandwidth of interest maps into the range of 0.95-9.5 Hz. Here, all the PSD calculations are performed using non-dimensional load coefficients, so the RMS quantities are non-dimensional as well. To convert the recorded time-histories to the frequency domain, Welch's algorithm is used [31]. The windowing of each segment results in reducing the noise in the spectral density estimate, at the expense of frequency resolution.

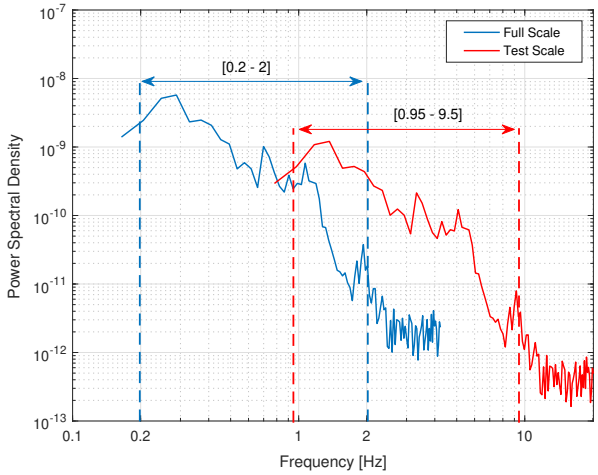

Figure 12: Illustration of the RMS loading calculation in full and test frequency scaling.

To compare the effect of wind direction, three test conditions are selected with the same free stream velocity but from different directions: HW, R30, and R60. Figures 13 compares this effect on the RMS values of thrust coefficient, for all test points along the stern trajectory and vertical offset. Figure 13 shows that in all three wind directions, the unsteadiness is increased while moving towards the landing point, where the maximum unsteadiness is experienced at P4, with 38%, 240%, and 231% increase with respect to P1 in HW, R30, and R60 respectively. Moving upward from this point, the unsteadiness is reduced in all wind conditions. This trend can be explained by looking at the topology of the flow field over the deck of the isolated SFS1, which is characterized by three main zones: recirculation, reattachment and re-developing regions. Figure 14 shows the flow field in the symmetry plane of the deck of the same ship model, visualized using PIV [27]. The position of the rotor at P4 was also shown in this figure with an altitude of about 60% of the hanger height. It can be seen that at P4, the rotor is immersed in the wake of the superstructure, especially the fore part of the rotor is significantly affected by the downwash due to the recirculation zone. This effect is reduced when the rotor is placed higher than

the height of the hangar wall which results in the reduction of the unsteadiness in the last three points along the vertical trajectory.

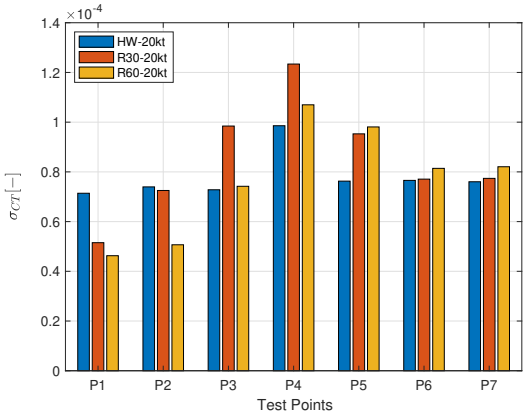

Figure 13: Effect of wind direction on unsteady thrust coefficient, comparison of HW, R30 and R60.

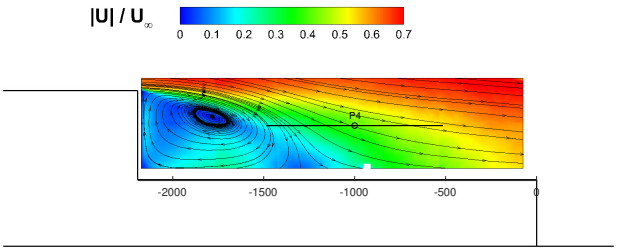

Figure 14: Contours of normalised in-plane velocity magnitude and streamlines in headwind $U_\infty = 4.8m/s$ [27]

With the wind coming from the port side, the initial part of the trajectory is less affected by the airwake of the ship than free stream flow, and this is more evident in R60 when the unsteadiness starts to rise particularly from P3. The comparison between P2 and P5, which are placed at the same height but different longitudinal positions with respect to the hangar wall, shows how more unsteadiness is involved in rotor inflow when it is placed at P5, the rate of increase is changed in different wind directions. In headwind, it shows only a

3% increase, while testing in R30 and R60, there is an increase of 31% and 93% respectively.

Variation of RMS moment coefficients is shown in Fig. 15. Both roll and pitch moments follow the same trend as observed in thrust. However, some differences can be appreciated as well. In the HW test, moving along the vertical path (P4 to P7) both moments do not show a noticeable reduction in unsteadiness with respect to the landing point (P4). Furthermore, in the same wind condition, the pitch moment at P2 has the highest unsteadiness which could be related to the asymmetric ground effect at this point, as the rotor is placed exactly above the stern edge. Thus, fore part of the rotor disk, which is above the deck, is more affected by the ground vortices compared to the aft part.

In R60, roll moment shows more unsteadiness compared with the pitch axis in all test points over the flight deck. This can be related to the spatial distribution of the turbulence intensity over the rotor disk which becomes more asymmetric in advancing and retreating side when the wind-angle increases towards the port or starboard side. Consequently, it can be expected that more unsteadiness is involved in roll moment while testing in R60.

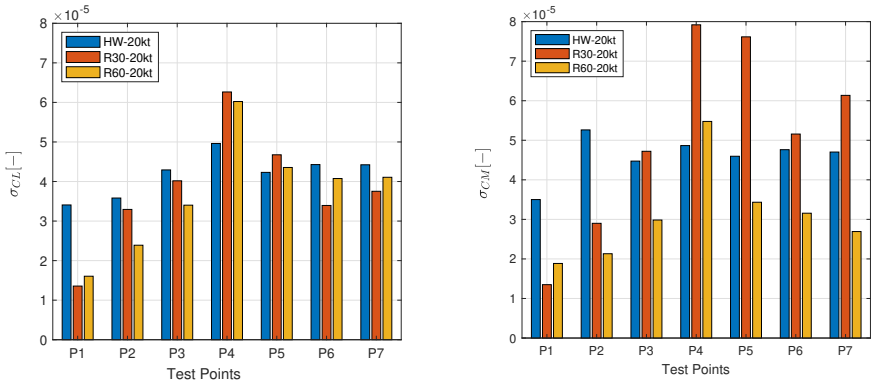

(a) Roll Moment

(b) Pitch Moment

Figure 15: Effect of wind direction on unsteady moment coefficient, comparison of HW, R30 and R60.

To compare the effect of wind speed, two free stream velocities in headwind

are selected. Figure 16 shows the variation of unsteadiness in aerodynamic loads, while free stream velocity is increased from 20 kt to 35 kt. Referring to Fig. 7, it can be seen that despite trimming the rotor in both wind speeds to obtain the same loads, the RMS values are increased in all three axes. For instance, a difference of 3% was observed in trimmed thrust coefficient at P1, while the increase of unsteadiness is 44%, as represented in Fig. 16(a). Figure 16 shows that the unsteadiness of thrust, roll, and pitch moments are increased in all test points. However, the initial point, P1, is less affected compared with those which are over the deck. The strong coupling between inflow of the rotor and airwake of the ship at these points results in a more turbulent flow field which reflects in a notable increase of RMS loading. Regarding the moments, as expected the pitch moment is more amplified with respect to the lateral one. In addition to the HW condition and lateral symmetry of the SFS1 geometry, variation of the moments unsteadiness could be also related to the stronger coupling between average and longitudinal inflow states of the rotor, so that the unsteadiness in thrust will affect the pitch moment more than the lateral one.

Another set of RMS values is presented in Fig.17 to see the effect of the dynamic approach on the unsteady loads. The total acquisition of 30 seconds is used to calculate the PSD of the measured loads, so that the RMS loading can be compared with the previous measurements at each point. To maintain the same trim objective as previous tests, the required trim controls in static tests were linearly combined to obtain the time history of the collective and cyclic commands during the dynamic approach. In this way, the trim condition of the rotor remains the same as the static tests and the effect of approach velocity can be evaluated on the unsteady loads.

Figure 17 shows the unsteady loading of the dynamic approach in comparison with the other 4 points of the trajectory. A weighted average of the unsteadiness obtained at each point has been calculated based on the fractions of total time spent between these four points. To have a better comparison with the dynamic test, this mean value is also presented in the fifth column. It can be seen that the weighted average of the unsteady thrust in both headwind

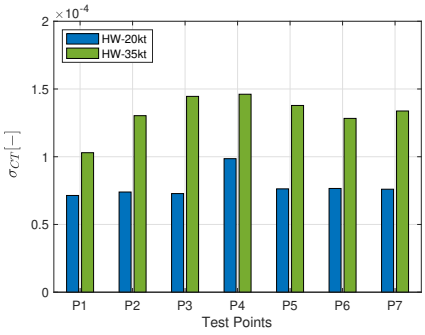

(a) Thrust

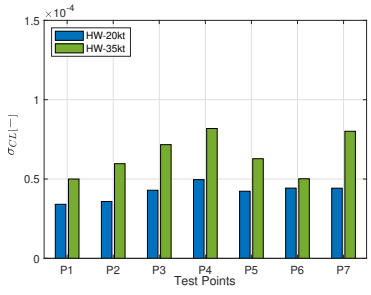

(b) Roll Moment

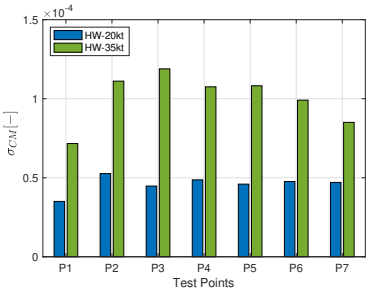

(c) Pitch Moment

Figure 16: Effect of wind velocity on unsteady loading in HW.

tests represents a fairly good correlation with the dynamic approach, as they both remain in a range of ±10% from the unsteadiness measured in the dynamic approach, while in Red30 the average of static measurements shows 15% less unsteadiness compared to the dynamic test. Regarding the in-plane moments, the unsteadiness of the roll moment in static and dynamic tests are very well correlated with less than 10% difference in all three wind directions. However, regarding the pitch moment, the averaged unsteadiness is higher than the one experienced during the dynamic test, especially in the headwind. Referring to Fig. 17(c), 8% and 19% differences can be observed in R30 and HW, where the wind speed is relatively low, while the difference is significantly increased to 67% for the HW test with the higher speed.

To verify that the trim condition of the rotor was maintained during the

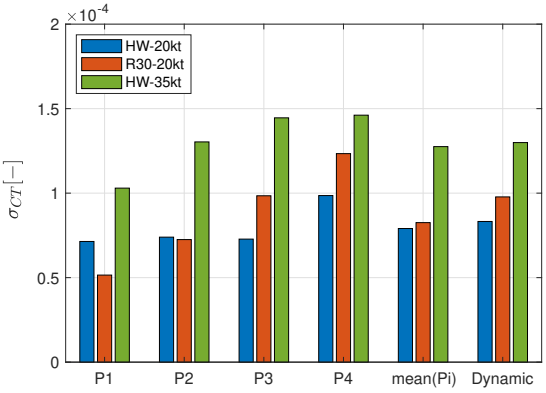

(a) Thrust

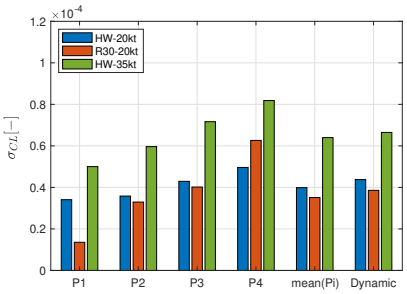

(b) Roll Moment

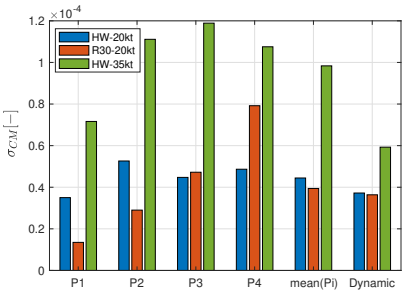

(c) Pitch Moment

Figure 17: Effect of approach velocity on the unsteady loading, comparison of static and dynamic tests.

dynamic test, time histories of the pitch moment in HW-35 kt are shown in Fig. 18, comparing the dynamic test and measurements at P1, P2, P3, and P4 in the same wind condition, and with the trim limits. The recorded time histories are filtered using a moving average filter with a window size of one second. It can be seen that near $t = 15$ s in the dynamic test, the mean value slightly increases and then reduces again towards zero. Referring to the trajectories presented in Fig. 6, at $t = 15sec$ the rotor is passing through the stern side of the deck, which results in changing the trim condition. However, the decreasing trend towards the last 5 seconds, which is the hovering time above the landing spot,

shows that the cyclic controls applied to the rotor were effective in keeping the longitudinal balance of the rotor plane. Notably, that the average value of the CM during 30 seconds of the dynamic test is 7.84×10^{-5}, which is well inside the accepted tolerance for trimming the moments in static tests. Comparing the time histories of the thrust and roll moment also confirms that the trim conditions were maintained during the dynamic test.

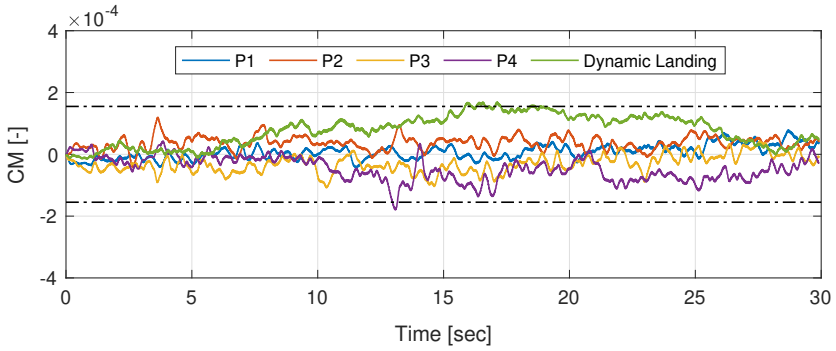

Figure 18: Time history of pitch moment coefficient-Comparison of dynamic test and static measurements.

The above comparisons indicate that the approach velocity positively reduces the unsteady pitching moment experienced by the rotor during the landing maneuver. Consequently, it can be inferred that using the static approach to obtain the operational limits through simulation may result in a higher workload for the pilot and a more conservative envelope compared to the flight test.

5. Conclusion

The aerodynamic loading of a scaled-helicopter operating in the airwake of a generic frigate model has been investigated through a series of wind tunnel tests. Time-averaged and unsteady rotor loads were measured for a range of wind speed, direction, and positions over the deck. A stern landing trajectory was defined as a sequence of points, starting from a position relatively far from the airwake of the ship, up to a point where the rotor is completely immersed in

the turbulent flow field created by the strong coupling between the rotor inflow and the ship airwake. Three additional points were also considered with vertical offset with respect to the landing spot. The rotor was placed at each point and trimmed for a constant level of thrust and zero in-plane moments through collective and cyclic pitch controls applied through the swashplate mechanism implemented in the model.

The variation of unsteady thrust and roll moment along the landing trajectory showed that in all wind conditions, the highest unsteadiness is experienced by the rotor at the lowest altitude and closest position to the hangar wall. Regarding the pitch moment in headwind, a slightly different trend was observed, as the unsteadiness remained relatively high in all the points over the deck. Furthermore, the variation of unsteadiness with wind speed was found to be affected by the interaction of the rotor inflow and ship airwake. Consequently, the rate of increment was changed at different points along the landing path.

Moreover, the effect of approach velocity on the unsteady loads was examined by performing a dynamic landing maneuver. Comparing the unsteadiness of dynamic tests with the measurements at fixed positions, confirmed a reasonable correlation in unsteady thrust and roll moment between two approaches. However, the unsteady pitch moment was found to decrease in dynamic landing. The reduction was especially notable while testing in headwind conditions and with higher wind speed. Consequently, assessment of the operational limits in DI simulation, based on the results of static approach may lead to overestimation of the pilot workload and impose unrealistic restrictions on the safe envelope of the operation.

Funding Sources

This research was supported by NITROS (Network for Innovative Training on ROtorcraft Safety) project which has received funding from the European Union's Horizon 2020 research and innovation program under the Marie Skłodowska-Curie grant agreement No. 721920.

References

[1] B. Lumsden, C. H. Wilkinson, G. D. Padfield, Challenges at the helicopter-ship dynamic interface, in: 24th European Rotorcraft Forum, 1998.

[2] A. Zanoni, M. Zago, R. Paolini, G. Quaranta, M. Galli, P. Masarati, On task dependence of helicopter pilot biodynamic feedthrough and neuromuscular admittance: An experimental and numerical study, IEEE Transactions on Human-Machine Systems (2021) 1–11doi:10.1109/THMS.2020.3044971.

[3] L. A. Hoencamp, M. D. Pavel, Concept of a predictive tool for ship–helicopter operational limitations of various in-service conditions, Journal of the American Helicopter Society 57 (3) (2012) 1–9. doi:10.4050/JAHS.57.032008.

[4] I. Owen, M. D. White, G. D. Padfield, S. J. Hodge, A virtual engineering approach to the ship-helicopter dynamic interface-a decade of modelling and simulation research at the university of liverpool, The Aeronautical Journal 121 (1198) (2013) 1233–1248. doi:10.1017/aer.2017.102.

[5] W. B. Greer, C. Sultan, Infinite horizon model predictive control tracking application to helicopters, Aerospace Science and Technology 98 (2020) 105675. doi:https://doi.org/10.1016/j.ast.2019.105675.

[6] Y. Huang, M. Zhu, Z. Zheng, M. Feroskhan, Fixed-time autonomous shipboard landing control of a helicopter with external disturbances, Aerospace Science and Technology 84 (2019) 18–30. doi:https://doi.org/10.1016/j.ast.2018.07.032.

[7] S. Abujoub, J. McPhee, R. A. Irani, Methodologies for landing autonomous aerial vehicles on maritime vessels, Aerospace Science and Technology 106 (2020) 106169. doi:https://doi.org/10.1016/j.ast.2020.106169.

[8] C. H. Wilkinson, G. M. VanderVliet, M. F. Roscoe, Modeling and simulation of the ship-helicopter environment, in: AIAA Modeling and Simulation Technologies Conference and Exhibit, Denver, USA, 2001.

[9] C. H. Wilkinson, M. F. Roscoe, G. M. VanderVliet, Determing fidelity standards for the shipboard launch and recovery task, in: AIAA Modeling and Simulation Technologies Conference and Exhibit, Montreal, Canada, 2001.

[10] D. M. Roper, I. Owen, G. D. Padfield, S. J. Hodge, Integrating cfd and piloted simulation to quantify ship-helicopter operating limits, The Aeronautical Journal 110 (1109) (2006) 419–428. doi:10.1017/S0001924000001329.

[11] C. Kääriä, J. Forrest, I. Owen, The virtual airdyn: a simulation technique for evaluating the aerodynamic impact of ship superstructures on helicopter operations, The Aeronautical Journal 117 (1198) (2013) 1233–1248.

[12] Y. Wang, J. Curran, G. D. Padfield, I. Owen, Airdyn: an instrumented model-scale helicopter for measuring unsteady aerodynamic loading in airwakes, Measurement Science and Technology 22 (4) (2011) 045901. doi:10.1088/0957-0233/22/4/045901.

[13] R. Thedin, S. M. Murman, J. Horn, S. Schmitz, Effects of atmospheric turbulence unsteadiness on ship airwakes and helicopter dynamics, Journal of Aircraft 57 (3) (2020) 534–546.

[14] S. J. Hodge, S. J. Zan, D. M. Roper, G. D. Padfield, I. Owen, Time-accurate ship airwake and unsteady aerodynamic loads modeling for maritime helicopter simulation, Journal of the American Helicopter Society 54 (2) (2009) 022005–1–16.

[15] D. T. McRuer, Interdisciplinary interactions and dynamic systems integration, International Journal of Control 59 (1) (1994) 3–12. doi:10.1080/00207179408923067.

[16] J. W. Bunnel, An integrated time-varying airwake in a uh-60 black hawk shipboard landing simulation, in: AIAA Modeling and Simulation Technologies Conference and Exhibit, Montreal, Canada, 2001.

[17] D. Lee, N. Sezer-Uzol, J. F. Horn, L. N. Long, Simulation of helicopter shipboard launch and recovery with time-accurate airwakes, Journal of Aircraft 42 (2) (2005) 448–461. doi:10.2514/1.6786.

[18] C. Crozon, R. Steijl, G. N. Barakos, Coupled flight dynamics and cfd – demonstration for helicopters in shipborne environment, The Aeronautical Journal 122 (1247) (2018) 42–82. doi:10.1017/aer.2017.112.

[19] J. F. Tan, T. Y. Zhou, Y. M. Sun, G. N. Barakos, Numerical investigation of the aerodynamic interaction between a tiltrotor and a tandem rotor during shipboard operations, Aerospace Science and Technology 87 (2019) 62–72. doi:https://doi.org/10.1016/j.ast.2019.02.005.

[20] I. Oruc, J. F. Horn, Coupled flight dynamics and computational fluid dynamics simulations of rotorcraft/terrain interactions, Journal of Aircraft 54 (6) (2017) 2228–2241. doi:10.2514/1.C034101.

[21] I. Oruc, J. F. Horn, J. Shipman, S. Polsky, Towards real-time pilot-in-the-loop cfd simulations of helicopter/ship dynamic interface, International Journal of Modeling, Simulation, and Scientific Computing 8 (4) (2017). doi:10.1142/S179396231743005X.

[22] S. J. Zan, Experimental determination of rotor thrust in a ship airwake, Journal of the American Helicopter Society 47 (2) (2002) 100–108. doi:10.4050/JAHS.47.100.

[23] R. G. Lee, S. J. Zan, Wind tunnel testing of a helicopter fuselage and rotor in a ship airwake, Journal of the American Helicopter Society 49 (2) (2004) 149–159. doi:10.4050/1.3092869.

[24] R. G. Lee, S. J. Zan, Wind tunnel testing of a helicopter fuselage and rotor in a ship airwake, Journal of the American Helicopter Society 50 (4) (2005) 326–337. doi:10.4050/1.3092869.

[25] C. H. Kääriä, Y. Wang, G. D. Padfield, J. S. Forrest, I. Owen, Aerodynamic loading characteristics of a model-scale helicopter in a ship's airwake, Journal of Aircraft 49 (5) (2012) 1271–1278. doi:10.2514/1.C031535.

[26] C. H. Kääriä, Y. Wang, M. D. White, I. Owen, An experimental technique for evaluating the aerodynamic impact of ship superstructures on helicopter operations, Ocean Engineering 115 (2021). doi:10.1016/j.oceaneng.2012.12.052.

[27] N. Taymourtash, D. Zagaglia, A. Zanotti, V. Muscarello, G. Gibertini, G. Quaranta, Experimental study of a helicopter model in shipboard operations, Aerospace Science and Technology 61 (2013) 97–108. doi:10.1016/j.ast.2021.106774.

[28] C. Wilkinson, S. J. Zan, N. E. Gilbert, J. D. Funk, Modelling and simulation of ship airwakes for helicopter operations: A collaborative venture, in: AGARD Symposium on Fluid Dynamics Problems of Vehicles Operating near or in the Air-Sea Interface, Amsterdam, The Netherlands, 1999.

[29] W. Cui, L. Caracoglia, Physics-based method for the removal of spurious resonant frequencies in high-frequency force balance tests, Journal of Structural Engineering 142 (2) (2016) 04015129. doi:10.1061/(ASCE)ST.1943-541X.0001414.

[30] J. V. Healey, Establishing a database for flight in the wakes of superstructures, Journal of Aircraft 29 (4) (1992) 559–564. doi:10.2514/3.46202.

[31] P. D. Welch, The use of fast fourier transform for the estimation of power spectra: A method based on time averaging over short, modified periodograms, IEEE Transactions on Audio and Electroacoustics 15 (2) (1967) 70–73. doi:10.1109/TAU.1967.1161901.